DNA damage repair profiling of esophageal squamous cell carcinoma uncovers clinically relevant molecular subtypes with distinct prognoses and therapeutic vulnerabilities

Ning Zhao,[a,f] Zicheng Zhang,[b,f] Qiang Wang,[c,f] Lin Li,[d,f] Zichao Wei,[a] Hongyan Chen,[a,e,**] Meng Zhou,[b,****] Zhihua Liu,[a,*] and Jianzhong Su[b,***]

[a]State Key Laboratory of Molecular Oncology, National Cancer Center/National Clinical Research Center for Cancer/Cancer Hospital, Chinese Academy of Medical Sciences and Peking Union Medical College, Beijing, 100021, PR China
[b]Oujiang Laboratory (Zhejiang Lab for Regenerative Medicine, Vision and Brain Health), Eye Hospital, Wenzhou Medical University, Wenzhou, 325027, PR China
[c]Department of Anesthesiology, National Cancer Center/National Clinical Research Center for Cancer/Cancer Hospital, Chinese Academy of Medical Sciences and Peking Union Medical College, Beijing, 100021, PR China
[d]Department of Pathology, National Cancer Center/ National Clinical Research Center for Cancer/Cancer Hospital, Chinese Academy of Medical Sciences and Peking Union Medical College, Beijing, 100021, PR China
[e]Key Laboratory of Cancer and Microbiome, National Cancer Center/ National Clinical Research Center for Cancer/Cancer Hospital, Chinese Academy of Medical Sciences and Peking Union Medical College, Beijing, 100021, PR China

eBioMedicine
2023;96: 104801
Published Online xxx
https://doi.org/10.1016/j.ebiom.2023.104801

Summary

Background DNA damage repair (DDR) is a critical process that maintains genomic integrity and plays essential roles at both the cellular and organismic levels. Here, we aimed to characterize the DDR profiling of esophageal squamous cell carcinoma (ESCC), investigate the prognostic value of DDR-related features, and explore their potential for guiding personalized treatment strategies.

Methods We analyzed bulk and single-cell transcriptomics data from 377 ESCC cases from our institution and other publicly available cohorts to identify major DDR subtypes. The heterogeneity in cellular and functional properties, tumor microenvironment (TME) characteristics, and prognostic significance of these DDR subtypes were investigated using immunogenomic analysis and *in vitro* experiments. Additionally, we experimentally validated a combinatorial immunotherapy strategy using syngeneic mouse models of ESCC.

Findings DDR alteration profiling enabled us to identify two distinct DDR subtypes, DDR^{active} and DDR^{silent}, which exhibited independent prognostic values in locoregional ESCC but not in metastatic ESCC. The DDR^{silent} subtype was characterized by an inflamed but immune-suppressed microenvironment with relatively high immune cell infiltration, abnormal immune checkpoint expression, T-cell exhaustion, and enrichment of cancer-related pathways. Moreover, DDR subtyping indicates that *BRCA1* and *HFM1* are robust and independent prognostic factors in locoregional ESCC. Finally, we proposed and verified that the concomitant triggering of *GITR* or blockade of *BTLA* with *PD-1* blockade or cisplatin chemotherapy represents effective combination strategies for high-risk locoregional ESCC tumors.

Interpretation Our discovery of DDR-based molecular subtypes will enhance our understanding of tumor heterogeneity and have significant clinical implications for the therapeutic and management strategies of locoregional ESCC.

Funding This study was supported by the National Key R&D Program of China (2021YFC2501000, 2022YFC3401003), National Natural Science Foundation of China (82172882), the Beijing Natural Science Foundation (7212085), the CAMS Innovation Fund for Medical Sciences (2021-I2M-1-018, 2021-I2M-1-067), the Fundamental Research Funds

*Corresponding author. State Key Laboratory of Molecular Oncology, National Cancer Center/National Clinical Research Center for Cancer/Cancer Hospital, Chinese Academy of Medical Sciences and Peking Union Medical College, Beijing, 100021, PR China.
**Corresponding author. State Key Laboratory of Molecular Oncology, National Cancer Center/National Clinical Research Center for Cancer/Cancer Hospital, Chinese Academy of Medical Sciences and Peking Union Medical College, Beijing, 100021, PR China.
***Corresponding author. Oujiang Laboratory (Zhejiang Lab for Regenerative Medicine, Vision and Brain Health), Eye Hospital, Wenzhou Medical University, Wenzhou, 325027, PR China.
****Corresponding author. Oujiang Laboratory (Zhejiang Lab for Regenerative Medicine, Vision and Brain Health), Eye Hospital, Wenzhou Medical University, Wenzhou, 325027, PR China.
E-mail addresses: liuzh@cicams.ac.cn (Z. Liu), chenhongyan@cicams.ac.cn (H. Chen), sujz@wmu.edu.cn (J. Su), zhoumeng@wmu.edu.cn (M. Zhou).
[f]Ning Zhao, Zicheng Zhang, Qiang Wang and Lin Li contributed equally to this work as first authors.

for the Central Universities (3332021091), and the Non-profit Central Research Institute Fund of Chinese Academy of Medical Sciences (2019PT310027).

Keywords: DNA damage repair; Esophageal squamous cell carcinoma; Immunotherapeutic targets; Tumor microenvironment

Research in context

Evidence before this study

Currently, no precise molecular biomarkers are available to predict the development of locoregional esophageal squamous cell carcinoma (ESCC) patients, resulting in limited clinical management options. Therefore, there is an urgent need to identify potential prognostic biomarkers for locoregional ESCC. Furthermore, no immunotherapies have been approved for locoregional ESCC, underscoring the need for a comprehensive understanding of the immune microenvironment to develop optimal immunotherapeutic approaches for locoregional ESCC patients. Recent evidence has highlighted the importance of DNA damage repair (DDR) deficiency in modulating the antitumor immune response. DDR deficiency can impact tumor antigenicity, adjuvanticity, and reactogenicity, ultimately influencing the efficacy of immunotherapy. However, the prognostic value of DDR-related features and their potential for guiding individualized treatment remains unclear for ESCC. Therefore, it is essential to elucidate the associations between alterations in the tumor DDR pathway and prognosis and develop personalized immunotherapy strategies based on DDR-specific characteristics.

Added value of this study

Our study utilized bulk and single-cell transcriptomics data from 377 patients to characterize the DDR landscape in ESCC. By analyzing DDR alterations, we identified two distinct DDR molecular subtypes, DDR^{active} and DDR^{silent}, which exhibited independent prognostic values in locoregional ESCC but not in metastatic ESCC. Additionally, DDR subtyping indicates that *BRCA1* and *HFM1* are robust and independent prognostic factors in locoregional ESCC. When cross-referencing alterations in the tumor immune microenvironment, we proposed and verified that the concomitant triggering of *GITR* or blockade of *BTLA* with *PD-1* blockade and cisplatin chemotherapy represent effective combination strategies for high-risk locoregional ESCC tumors.

Implications of all the available evidence

Comprehensive characterization and understanding of the DDR landscape in ESCC provide essential insights into the prognosis and clinical management of locoregional ESCC patients. Identifying DDR subtypes and their independent prognostic values can facilitate a more precise disease categorization, potentially allowing for personalized treatment strategies based on DDR-specific characteristics.

Introduction

Esophageal squamous cell carcinoma (ESCC) is a malignant tumor that threatens human health, with a five-year survival rate of less than 20% in developed countries and less than 5% in many developing countries.[1] It is worth noting that some locoregional ESCC patients often relapse rapidly after esophagectomy, and the prognosis of these patients remains poor.[2] To date, no precise molecular biomarkers can predict the development of these locoregional ESCC patients, leading to poor clinical management. Hence, it is urgent to identify potential prognostic biomarkers for locoregional ESCC.[3,4]

DNA damage repair (DDR) is a critical process that maintains genomic integrity and plays essential roles at both the cellular and organismic levels. It involves a complex network of pathways and mechanisms, including homologous recombination (HR), non-homologous end-joining (NHEJ), mismatch repair (MMR) and nucleotide excision repair pathways (NER).[5] DDR deficiency results in the accumulation of DNA damage and genomic instability, the generation of neoantigens and the upregulation of the expression of immune checkpoints, ultimately altering the immune balance in the tumor microenvironment (TME).[6–8] Interestingly, DDR deficiency has recently emerged as an important determinant of the antitumor immune response by affecting antigenicity, adjuvanticity and reactogenicity, which may contribute to the response to immunotherapy.[9] Recent studies have revealed the potential of some DDR-based biomarkers in predicting clinical outcome and the response to immunotherapy.[10–14] Therefore, understanding the DDR profile in specific cancers can provide valuable insights into the underlying molecular mechanisms and identify potential prognostic markers and therapeutic targets. However, the value of DDR-related features for prognosis evaluation and individualized immunotherapy has not been fully elucidated in ESCC.

In this study, we utilized transcriptome profiles and clinicopathological information from 377 patients to characterize the DDR landscape in ESCC. The DDR subtyping showed a heterogeneous immune infiltrated

phenotype at the transcriptomic level. Furthermore, we demonstrated that *BRCA1* and *HFM1* were maintenance and suppression factors for the DDR system in ESCC cell lines. We provided extensive evidence of independent prognostic factors for *BRCA1* and *HFM1*. Cross-reference with the alteration of tumor immune microenvironment further revealed a potential new immunotherapy strategy. Strikingly, we discovered and experimentally validated a combinatorial immunotherapy strategy for DDR subtype-specific locoregional ESCC patients.

Methods

Study population and patient cohorts

Our study included cohorts of ESCC patients from the Shanxi Cancer Hospital (SCH cohort, a total of 155 patients with RNA-seq data) from our previous study,[15] The Cancer Genome Atlas (TCGA-ESCC cohort, a total of 74 ESCC patients with RNA-seq data), and the Chinese Academy of Medical Sciences and Peking Union Medical College (Chen cohort, a total of 117 ESCC patients with microarray data and Zhang cohort, a total of 31 locoregional ESCC patients with scRNA-seq data).

RNA-seq data of the SCH cohort were obtained from Genome Sequence Archive (GSA) in the BIG Data Center (http://bigd.big.ac.cn/gsa), Beijing Institute of Genomics (BIG), Chinese Academy of Sciences, with the BioProject number PRJCA004501. RNA-seq data profiling of the TCGA cohort were collected from the UCSC Xena browser (https://xenabrowser.net/datapages/). The RNA-seq data were normalized to the TPM level and log2 (x + 1) in our study. Gene expression profiling by the Agilent human lncRNA + mRNA array V.2.0 platform and clinical data of the Chen cohort was downloaded from the Gene Expression Omnibus (GEO, www.ncbi.nlm.nih.gov/geo/query/acc.cgi?acc=GSE53624).[16] Single-cell transcriptomes of the Zhang cohort were downloaded from the GEO (https://www.ncbi.nlm.nih.gov/geo/query/acc.cgi?acc=GSE160269).[17] The main characteristics of the study populations are summarized in Table 1 and Supplementary Table S1.

Cell lines and cell culture

The human ESCC cell lines KYSE30 (CVCL_1351), KYSE410 (CVCL_1352) and KYSE450 (CVCL_1353) were provided by Dr. Yutaka Shimada (Kyoto University, Kyoto, Japan) and cultured in RPMI-1640 medium supplemented with 10% fetal bovine serum (FBS). The mouse ESCC cell line mEC25 (CVCL_C6JH) was a gift from Li Fu Laboratory (Shenzhen, China) and cultured in DMEM supplemented with 10% FBS.[18] All cells were maintained in a humidified cell incubator with 5% CO_2 at 37 °C and routinely authenticated using short tandem repeat (STR) DNA fingerprinting. Cells were assessed by a MycoBlue Mycoplasma Detector (Vazyme Biotech, Nanjing, China) to exclude Mycoplasma contamination before experiments.

DDR subtype classification

An expert-curated 268-gene list of six major DDR pathways, including base excision repair (BER, n = 43), mismatch repair (MMR, n = 27), nucleotide excision repair (NER, n = 70), Fanconi anemia (FA, n = 36), homologous recombination (HR, n = 55) and nonhomologous end-joining (NHEJ, n = 37), was obtained from Pearl et al.[5] We performed consensus clustering analysis to determine the optimal number of stable DDR-based ESCC subtypes based on the expression profiles of specific DDR genes. This clustering procedure was conducted using the R package ConsensusClusterPlus with 1000 iterations and 90% resampling.[19]

Molecular characterization of DDR subtypes

To characterize the DDR subtypes, we performed differential expression analysis between DDR subtypes to determine subtype-specific genes using the R package limma (V3.50.3).[20] Differentially expressed genes (DEGs) were defined as genes with a log-fold change (logFC) ≤ -1 or ≥ 1 and an adjusted P value < 0.05. We then performed pathway enrichment analysis on DEGs for a curated set of hallmark pathways from the Molecular Signatures Database (MSigDB)[21] to identify enriched pathways in DDR subtypes, as implemented by the R package ClusterProfiler (V4.2.2).[22]

Characterizing the cellular and functional properties of the TME by DDR subtyping

To characterize the cellular and functional properties of the TME by DDR subtyping, we referred to a previous study to obtain 29 knowledge-based functional gene expression signatures (Fges) covering known immune, stromal, and other major cellular functional components of the tumor. We then conducted single sample gene set enrichment analysis (ssGSEA) on these 29 Fges to generate enrichment scores as the activated index for each pathway in each sample, as implemented by the R package GSVA (V1.42.0).[23]

To characterize the immune infiltration landscape of DDR subtypes, the tumor infiltration levels of diverse immune cell types were quantified computationally using single-sample gene set enrichment analysis (ssGSEA) based on 28 immune cell gene signatures curated from previous studies.[24,25] T-cell exhaustion (TEX) states in the TME were assessed based on published TEX gene signatures[26] using ssGSEA.

Single-cell data analysis

Single-cell RNA-seq data for 32,918 T cells from 31 locoregional ESCC patients were downloaded from GEO (GSE160269). Principal component analysis (PCA) (50 principal components) of ScaleData of these T-cell UMI counts was calculated on 2000 highly variable genes (HVGs), which were identified by the variance-stabilizing transformation (vst) selection method, and the top 30/50 principal components were used for

	SCH cohort (n = 155)	TCGA-ESCC cohort (n = 74)	Chen cohort (n = 117)
OS state			
Alive	48	54	46
Dead	49	20	71
Unknown	58	0	0
N info			
0	82	46	53
1	41	21	41
2	22	5	13
3	10	1	10
Unknown	0	1	0
Grade			
Higher	133	–	–
Lower	22	–	–
Sex			
Male	103	63	97
Female	52	10	20
Unknown	0	1	0
Age			
>60	92	26	48
≤60	63	48	69

Table 1: **Baseline patient characteristics of the different cohorts.**

t-distributed stochastic neighbor embedding (t-SNE) dimensionality reduction by the RunTSNE function in Seurat.[27] The T cells were determined for seven subtypes at a clustering resolution of 0.15. All cells in the specific cluster were compared with the rest of the cell types in the data by the 'FindAllMarkers' function to display the differentially expressed genes (DEGs) for each particular cell type with the threshold of 0.5 of logFC. Cell markers of each cluster were obtained from the CellMarker database (http://xteam.xbio.top/CellMarker/) and a previous study.[17]

SiRNA transfection

SiRNA pools were purchased from JTSBIO. KYSE30, KYSE410 and KYSE450 cells were plated in 6-well plates, and transfections were performed with siRNAs at -a final concentration of 60 nM using Hieff TransTM Liposomal Transfection Reagent (YENSEN) according to the manufacturer's instructions. The sequences of the siRNA pools used were as follows: SiBRCA1: GGAUGAAA UCAGUUUGGAU; CCUUCUAACAGCUACCCUU; CCACACGAUUUGACGGAAA; SiHFM1: CCUCCUG-CUCCAUUGAUUU; GAACAAAGAUGGAAUUGAA; CCGAGAAUGCAAUCAUCUU; SiNC: UUCUCCGAA-CGUGUCACGU.

Protein extraction and western blotting

KYSE30, KYSE410 and KYSE450 cells were treated with cisplatin (2 μg/ml) or exposed to 4 Gy X-ray irradiation (X-IR) after transfection for 48 h. Cells were lysed in RIPA lysis buffer (CWBIO, Beijing, China) supplemented with protease and phosphatase inhibitors (Roche, Basel, Switzerland). Proteins were quantified by the Pierce BCA Protein Assay Kit (Thermo Fisher Scientific). The proteins were then separated by SDS-polyacrylamide gel electrophoresis (SDS/PAGE) and transferred onto polyvinylidene difluoride membranes (Merck Millipore, Billerica, MA, USA). The membranes were blocked with 5% nonfat milk and probed with antibodies (HFM1: Thermo Fisher, PA5-109810, AB_2855221; BRCA1: Proteintech, 22362-1-AP, AB_2879090) overnight at 4 °C. Horseradish peroxidase-conjugated secondary antibodies (1:5000) and substrate was used to detect protein abundance according to the manufacturer's instructions. Western blot images were acquired by an ImageQuant LAS-4000 System.

Immunofluorescence

KYSE410 and KYSE450 cells were planted on coverslips and μ-slide VI coverslips (ibidi, Germany) at 24 h after transfection. Cells were incubated overnight and subsequently treated with cisplatin (2 μg/ml) or exposed to 4 Gy X-IR. After being fixed with paraformaldehyde and permeabilized with Triton X-100, the cells were blocked with 3% BSA and then incubated with γ-H2AX (Cell Signaling Technology, 80312, AB_2799949) antibodies overnight. Anti-mouse IgG conjugated with Alexa Fluor 488 (Proteintech, SA00013-5, AB_2890971) was used to detect the protein signal. After incubation with a fluorescent mounting medium with DAPI (4, 6-diamidino-2-phenylindole) (ZSGB-BIO, ZLI-9557) for 5 min, the cells were visualized with a laser confocal microscope.

Mice and *in vivo* treatments

All mouse procedures were performed in accordance with protocol guidelines approved by the Animal Care

and Use Committee of the Chinese Academy of Medical Sciences Cancer Hospital (NCC2021A281). Six-week-old female C57BL/6 mice were purchased from Charles River Laboratories (Beijing, China). Mice were bred and kept in animal housing facilities. mEC25 cells (4×10^6 cells per mouse) in Matrigel (356,237, Corning) were implanted subcutaneously into C57BL/6 mice. Mice were randomly assigned to treatment groups using the hierarchical random grouping method when most tumors grew approximately 5 mm in diameter. Mice were treated every three days by intraperitoneal injection of 100 μg DDP, anti-GITR (clone DTA-1, Bio X Cell, BE0063, AB_1107688), anti-BTLA (clone 6A6, Bio X Cell, BE0132, AB_10949299), anti-PD-1 (clone RMP1-14, Bio X Cell, BE0146, AB_10949053), anti-GITR plus anti-PD-1, anti-BTLA plus anti-PD-1, anti-GITR plus DDP, anti-BTLA plus DDP, saline or isotype control IgG (rat IgG2b, clone LTF-2, BE0090, AB_1107780; Armenian hamster IgG, clone Polyclonal, BE0091, AB_1107773; rat IgG2a, clone 2A3, BE0089, AB_1107769; Bio X Cell). Mice were treated and tumors were measured at the same time by one person. Mice cages were placed next to each other. If the tumor was larger than 1 cm in length or reached the end of the study, mice were asphyxiated by carbon dioxide.

The evaluation of tumor-infiltrating lymphocytes (TILs)

The levels of TILs in murine tumor tissues were assessed by hematoxylin and eosin (H&E)-stained tumor sections. The percentage of stromal TILs is determined by the percentage of the area occupied by mononuclear inflammatory cells over total intratumoral stromal area.

Flow cytometry analysis

C57BL/6 mice transplanted with mEC25 cells were treated twice with anti-GITR, anti-BTLA or their respective isotype control. Tumor tissues were dissected, minced and digested with 5 mg/ml collagenase Type I (17100017; ThermoFisher) at 37 °C for 30 min. The isolated cells were passed through a 70 μm filter, centrifuged at 500 g for 10 min at 4 °C, and the supernatant was discarded. The cells were precipitated and resuspended in Red Blood Cell Lysis Buffer (R1010, Solarbio) to remove red blood cells. The remaining cells were suspended in a staining buffer (Biolegend, 420201) and blocked with anti-CD16/CD32 antibodies (Tonbo, 70-0161-M001, AB_2621487) at room temperature for 30 min. Cells were stained with zombie (BioLegend, 423106) for 10 min. Cells were then stained with anti-CD45 (BioLegend, 103138, AB_2563061), anti-CD3 (100305, BD Biosciences, AB_312670), anti-CD8 (100734, BioLegend, AB_2075238) and anti-CD279 (100734, BioLegend, AB_1877232) antibodies for 45 min on ice. CD8+ PD1+(CD279+) T cells in CD8+ cells were defined as exhausted T cells. All flow samples were run on the LSR Fortessa (BD) system and data were analysed by FlowJo (v.10).

Statistical analysis

The statistical analyses were performed, and graphs were generated with GraphPad Prism version 8.0.1 (San Diego, CA, USA), and other analyses were performed using R (V4.1.1) based on the RStudio (V1.4.1717) workbench. Each experiment was performed at least three times, and quantitative data are shown as the mean ± SD. Mann–Whitney U test was used to compare differences between two independent groups, and the Kruskal–Wallis test was used for comparing more than two groups. The Kaplan–Meier method generated survival curves for the patient subgroups, and log-rank testing was used to determine the survival differences. Univariable and multivariable Cox proportional hazard regression models adjusted or not adjusted for available clinical covariates were used to calculate hazard ratios (HRs) and 95% confidence intervals (CIs), with time-to-event as the time scale. Individuals were censored at death or the date of follow-up. The proportional hazard assumption was assessed and met using Schoenfeld residuals with the coxph () function in the survival R package. Two-sided P values of less than 0.05 were considered to indicate statistical significance.

Role of funders

The funders were not involved in the study design, data collection, data analysis, interpretation or writing of the manuscript.

Results

Profiling of DDR pathways identified DDR subtypes that were prognostically independent of clinical variables in locoregional ESCC

We conducted RNA-seq on tumor tissues from 82 locoregional ESCC patients and 73 ESCC patients with lymph node metastasis (LNM). To determine the association between DDR pathways and ESCC patient survival in detail, we built a compendium of six DDR pathways and 268 corresponding genes from Pearl et al.[5] (Supplementary Table S2). and calculated a patient–level activity score for each DDR pathway using ssGSEA based on the pathway gene set. Then, we conducted univariable Cox regression analysis and observed that four of six DDR pathways (MMR, NER, FA, and HR pathways) were significantly associated with improved survival (Figure S1a). Therefore, we leveraged the expression profiles of 151 genes from four DDR pathways to group all 155 patients from the SCH cohort using consensus clustering and identified DDR clusters that differed in their survival outcomes (Fig. 1a and b, and Figure S1b). The DDR-active (referred to as DDR^{active}) cluster was associated with improved survival, and the DDR-silent (referred to as DDR^{silent}) cluster was associated with poor survival (HR = 0.483, 95% CI 0.268–0.872, log-rank P = 0.014) (Fig. 1b). Next, we also conducted stratification analysis to investigate

the correlations between DDR subtyping and survival for ESCC with and without LNM. The results showed that locoregional ESCC tumors in the DDR^{silent} subtype had the worst survival compared to locoregional ESCC tumors in the DDR^{active} subtype and metastatic ESCC tumors (log-rank P = 0.032) (Fig. 1c), but no significant survival difference was observed between DDR subtypes for metastatic ESCC tumors (log-rank P = 0.34) (Fig. 1d and Figure S1c). To further validate the association between the DDR subtype and survival outcome, we performed DDR subtyping in the TCGA-ESCC cohort (74 patients) and the Chen cohort (117 patients) (Figure S1d). In line with findings for our cohort, we observed that DDR subtyping assisted in survival prediction only for patients with locoregional ESCC tumors, allowing the identification of patient subgroups with good or poor outcomes (HR = 0.075, 95% CI 0.008–0.674, log-rank P = 0.004 for the TCGA-ESCC cohort and HR = 0.430, 95% CI 0.186–0.995, log-rank P = 0.042 for the Chen cohort) (Fig. 1e) and was unable to stratify ESCC patients with LNM based on survival (Figure S1e). Multivariable Cox regression analysis showed that the DDR subtype was a robust prognostic indicator independent of clinical variables, highlighting the value of DDR subtyping and its robustness in predicting survival outcomes in locoregional ESCC patients (Figure S1f).

DDR subtyping indicates that BRCA1 and HFM1 are robust and independent prognostic factors in locoregional ESCC

Given the above observation that the activation of DDR pathways has a context-dependent prognostic impact that differs between ESCC with and without LNM, we further assessed the prognostic effect of 151 genes from four DDR pathways on locoregional ESCC patients and observed that eight DDR genes were significantly associated with survival outcome using the univariable Cox regression model (Fig. 2a). In multivariable analyses controlled for sex, grade, smoking history and drinking history, only two DDR genes, *BRCA1* (breast cancer 1) and *HFM1* (helicase for meiosis 1), still maintained a significant association with survival outcome (Fig. 2a). We then used a meta-analysis to leverage three independent ESCC cohorts for an overall prognosis evaluation based on three DDR genes in locoregional and metastatic ESCC tumors and observed that only *BRCA1* and *HFM1* are robust prognosticators of survival outcome for locoregional ESCC across multicenter cohorts (Fig. 2b) but had no contribution to prognosis in metastatic ESCC (Figure S2a). *BRCA1* was identified as a favorable prognostic factor, and its high expression was associated with improved survival with a pooled HR of 0.060, 0.114 and 0.390; *HFM1* was a risk factor, and its increased expression was associated with poor survival outcome with a pooled HR of 5.050, 4.549, 3.520 across different cohorts (Fig. 2c–e).

BRCA1 promotes DDR, while HFM1 suppresses DDR in ESCC cells

BRCA1 plays an essential role in DDR. In the presence of BRCA1, cells sense and repair DNA lesions, which sustains genomic integrity and prevents tumorigenesis.[28] BRCA1 deficiency disrupts normal DDR and results in the accumulation of DNA damage. However, the role of HFM1, an ATP-dependent DNA helicase homolog in DDR, has not yet been widely studied.[29] To determine the roles of BRCA1 and HFM1 in DDR in ESCC cells, we constructed a cell model of cisplatin (DDP) and X-IR-induced DNA damage *in vitro*. We selected cell lines with high expression levels of BRCA1 or HFM1 and depleted BRCA1 or HFM1 using transient siRNA transfection and treated cells with cisplatin (DDP) or X-IR. The knockdown efficiency of BRCA1 and HFM1 was detected by Western blotting (Fig. 3a, b, e and f). To directly assess DDR, γH2AX, a well-established DNA DSB marker, was visualized by immunofluorescence. Spontaneous and DDP- or IR-induced foci for γH2AX were counted and analyzed. After DDP or X-IR treatment, γH2AX accumulated. Moreover, immunofluorescence analysis showed that endogenous γH2AX accumulation significantly increased after BRCA1 knockdown upon IR and DDP treatment in KYSE410 and KYSE450 cells (Fig. 3c and d). In contrast, the knockdown of HFM1 significantly decreased the number of γH2AX foci in both KYSE30 and KYSE450 cells treated with X-IR or DDP (Fig. 3g and h). These results demonstrated that loss of BRCA1 resulted in DDR defects, which supports the role of BRCA1 as a favorable prognostic factor, whereas loss of HFM1 promoted DDR, supporting the role of HFM1 as a prognostic risk factor.

TME characterization of DDR subtypes identified GITR and BTLA as potential immunotherapeutic targets in high-risk locoregional ESCC patients

As DDR subtyping displayed prognostic value in locoregional ESCC tumors, we reclustered only 82 locoregional tumors from the SCH cohort based on gene expression in four DDR pathways and used the consensus clustering algorithm (Figure S3a). The resulting three clusters (DDR subtypes termed DDR^{active}, $DDR^{moderate}$ and DDR^{silent}) were characterized by gradually decreasing activities of DDR pathways (Fig. 4a) and showed distinct survival outcomes (Fig. 4b). To determine the main biological features and underlying DDR subtypes, we performed pathway-level comparison analysis across DDR subtypes by performing GSEA of MSigDB hallmark pathways and observed that DDR^{silent} tumors were enriched not only in immune response-related pathways, including allograft rejection, coagulation, and complement pathway IFN-γ response, IL6/JAK/STAT3 signaling, inflammatory response, IL-2–STAT5 signaling, TNFA signaling via NFKB but also in canonical cancer-related pathways, including KRAS signaling, P53 pathway, apoptosis,

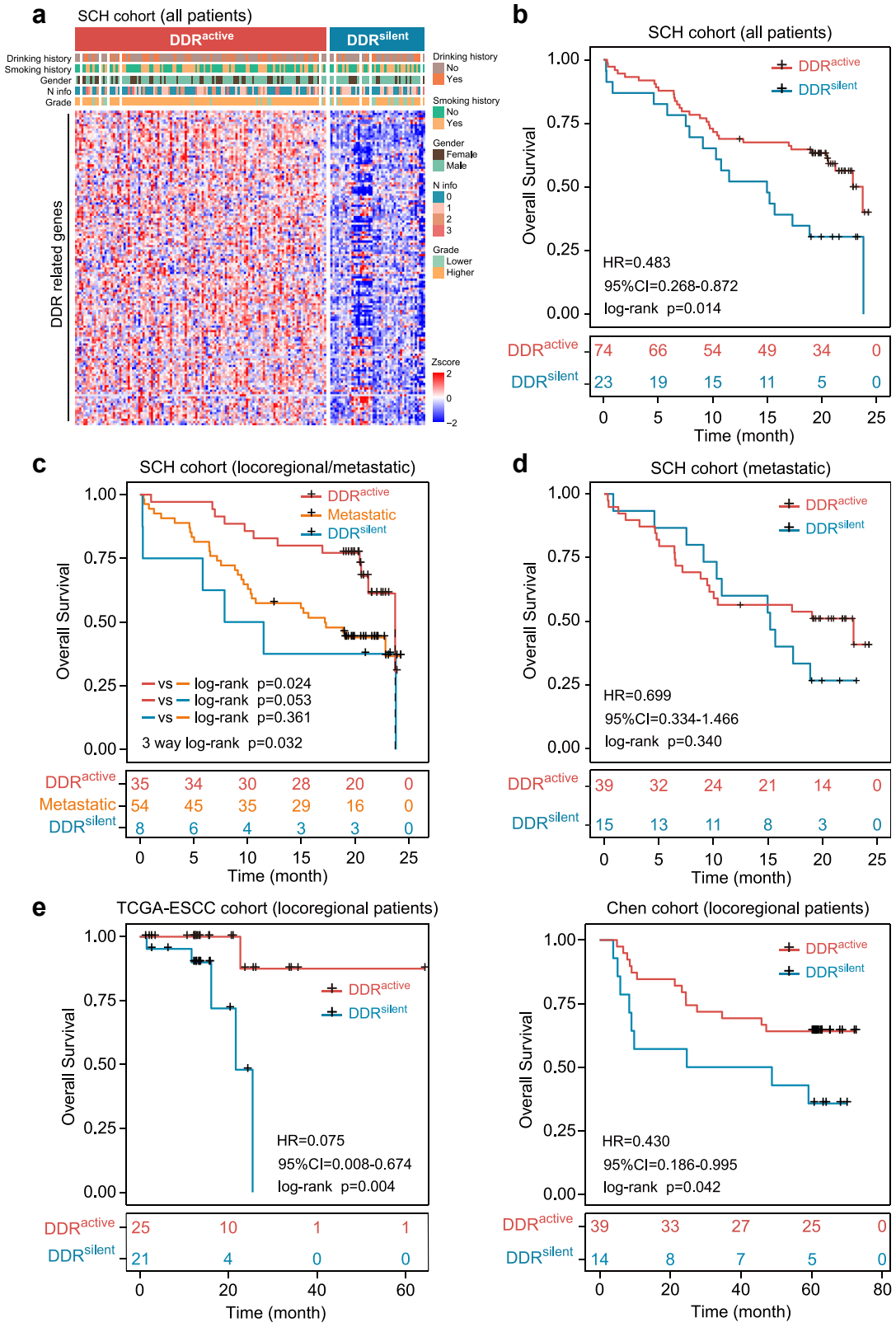
a
SCH cohort (all patients)
DDRactive
DDRsilent
Drinking history
Smoking history
Gender
N info
Grade
DDR related genes
Zscore
b
SCH cohort (all patients)
Overall Survival
HR=0.483
95%CI=0.268-0.872
log-rank p=0.014
Time (month)
c
SCH cohort (locoregional/metastatic)
Metastatic
vs log-rank p=0.024
vs log-rank p=0.053
vs log-rank p=0.361
3 way log-rank p=0.032
d
SCH cohort (metastatic)
HR=0.699
95%CI=0.334-1.466
log-rank p=0.340
e
TCGA-ESCC cohort (locoregional patients)
HR=0.075
95%CI=0.008-0.674
log-rank p=0.004
Chen cohort (locoregional patients)
HR=0.430
95%CI=0.186-0.995
log-rank p=0.042

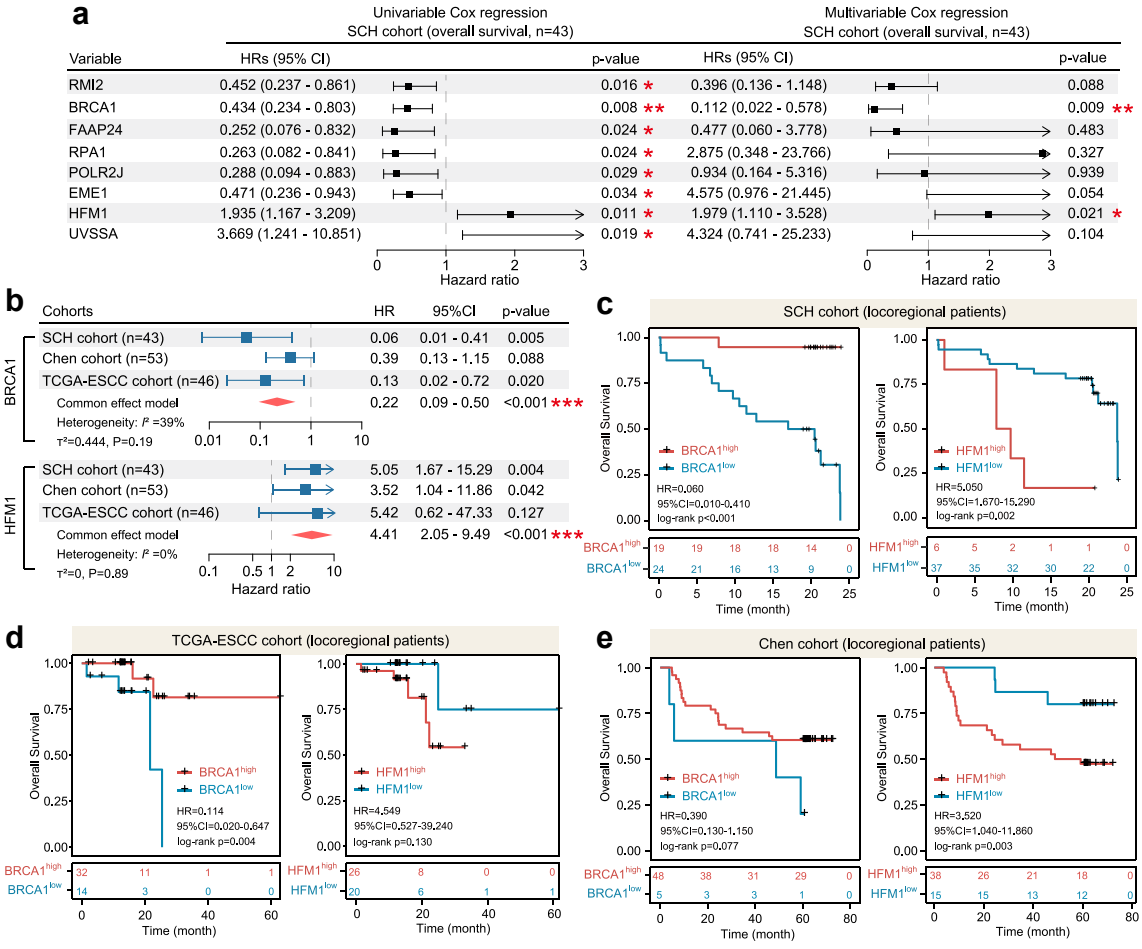

***Fig. 2:* BRCA1 and HFM1 are independent prognostic factors in** locoregional **ESCC.** (a) Forest plot showing the univariable and multivariable Cox regression analysis of eight significant prognostic DDR genes and clinicopathological features based on OS in the SCH cohort with a two-sided Wald test. The box represents HR, and the vertical bar represents ±95% CIs. (b) Forest plots of a meta-analysis showing the robust prognostic effect in three cohorts for prognostic DDR genes. The box represents HR, and the vertical bar represents ±95% CIs. The red diamond represents the common effect model of the meta-analysis. (c–e) Kaplan–Meier curves comparing OS between high BRCA1 and low BRCA1 and high HFM1 and low HFM1. The HRs and 95% CIs were calculated by a two-sided Wald test using univariable Cox regression.

epithelial–mesenchymal transition, while DDR^{active} tumors were enriched in cell proliferation-related gene sets, including E2F targets, G2M checkpoint, MYC targets v1 and v2 (Fig. 4c and d). These results indicated that tumors of different DDR subtypes display differences in cellular functions and the TME.

To further characterize the heterogeneity of cellular and functional TME properties of DDR subtyping, we scored 29 knowledge-based functional gene expression signatures (Fges) covering known immune, stromal, and other major cellular functional components of the tumor using ssGSEA and observed that these DDR subtypes

***Fig. 1:* Clustering analysis of ESCC tumors based on DDR gene profiles.** (a) Heatmap of the expression fold changes in DDR genes between DDR subtypes. The red bar represents the DDR^{active} subtype, and the green bar represents the DDR^{silent} subtype. The DDR subtypes are classified by the consensus clustering method. (b) Kaplan–Meier curves comparing OS between DDR^{active} subtype and DDR^{silent} subtype for all ESCC patients. (c) Kaplan–Meier curves comparing OS among the locoregional ESCC DDR^{active} subtype, locoregional ESCC DDR^{silent} subtype and metastatic ESCC tumors. (d) Kaplan–Meier curves comparing OS between DDR^{active} subtype and DDR^{silent} subtype only for metastatic ESCC patients. (e) Kaplan–Meier curves comparing OS between DDR^{active} subtype and DDR^{silent} subtype only for locoregional ESCC patients in TCGA-ESCC cohort and Chen cohort.

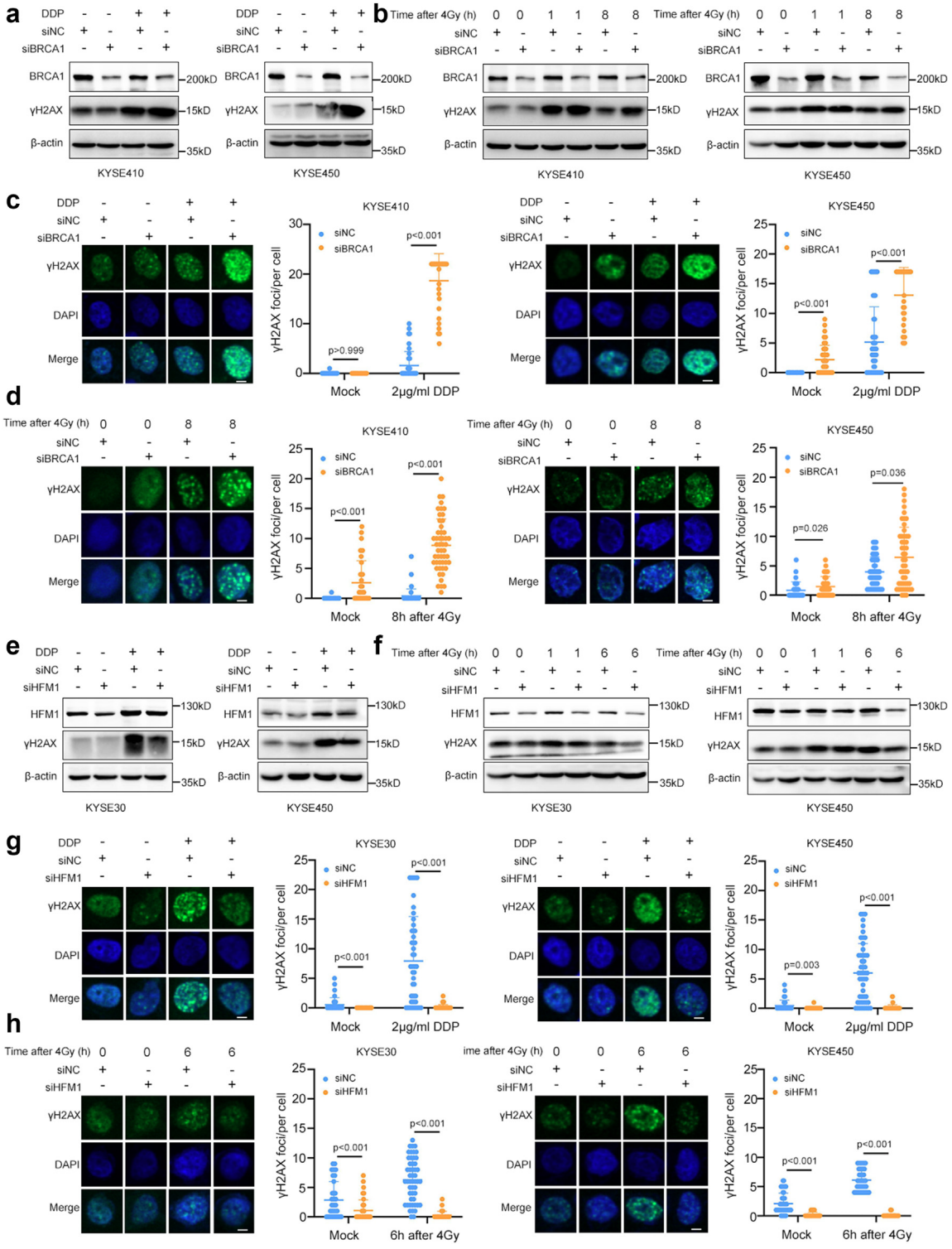

Fig. 3: **BRCA1 promotes DDR, while HFM1 suppresses DDR in ESCC cells.** (a) KYSE410 and KYSE450 cells were transfected with siRNAs targeting BRCA1 and control siRNAs and then treated with 2 μg/ml DDP. The expression of BRCA1 and γH2AX was analyzed by Western blotting. (b) KYSE410 and KYSE450 cells were transfected with siRNAs targeting BRCA1 and control siRNAs, exposed to X-IR (4 Gy), and harvested at the indicated times. The expression of BRCA1 and γH2AX was analyzed by Western blotting. (c, d) Representative pictures and quantification analysis of γH2AX foci in BRCA1-depleted KYSE410 and KYSE450 cells and control cells treated with 2 μg/ml DDP (c) or X-IR

varied significantly based on the expression of the 29 Fges (Fig. 4e). DDR^{silent} tumors were distinguished by significantly increased immune infiltration compared to the other two DDR subtypes (Fig. 4e). Differences in the immune microenvironment between the DDR subtypes were also observed when analyzing the previously reported abundance of 28 tumor-infiltrating immune cells using bulk-seq data and ssGSEA (Figure S3b). To determine why DDR^{silent} tumors with high immune infiltration have the worst prognosis, we examined the T-cell exhaustion status based on previously reported TEX-related signatures and ssGSEA and observed that DDR^{silent} tumors displayed significantly higher enrichment scores of TEX signal gene sets than the other two DDR subtypes (Fig. 4f). We further compared the expression levels of immunomodulators (including costimulatory and immune checkpoint molecules) among subtypes and found that DDR^{silent} had a higher expression of immune checkpoint molecules (PD-1 and BTLA) and a lower expression of a costimulatory molecule (GITR) (Figures S4g and S3c). These findings suggest that DDR^{silent} tumors may exhibit an inflamed but immune-suppressed microenvironment, as indicated by high immune cell infiltration, elevated immune checkpoint expression and T-cell exhaustion.

To further characterize the gene expression states of *PD-1*, *BTLA*, and *GITR* in the T-cell compartment involved in ESCC at the single-cell resolution, a total of 32,918 T cells were collected from 31 locoregional ESCC patients.[17] We initially identified seven T-cell subpopulations based on their canonical gene markers; these subpopulations included T helper 17, cytotoxic T cells, NK T cells, exhausted CD8 T cells, memory CD8 T cells, naïve T cells, and regulatory CD4 T cells (Fig. 4h). The regulatory CD4 T-cell subpopulation was marked by transcripts including *CD4*, *IL32*, *FOXP3*, and *IL2RA* (Fig. 4i). There were typical exhaustion markers, including *TOX*, *CTLA-4*, *TIGIT* and *CXCL13*, in the exhausted CD8 T-cell subpopulation, and the cytotoxic T-cell subpopulation was marked by high expression of *GNLY*, *GZMA*, *GZMB* and *NKG7* (Fig. 4i). As shown in Fig. 4j, *GITR* was highly expressed in regulatory CD4 T cells and cytotoxic T cells. In contrast, *BTLA* and *PD-1* were expressed in many T-cell subpopulations, including exhausted T cells. Thus, the complementary transcriptional status of *PD-1* and *GITR* and the similar transcriptional status of *PD-1* and *BTLA* among T-cell subpopulations observed in locoregional ESCC patients indicate that DDR^{silent} tumors may be responsive to concomitant *BTLA* blockade or *GITR* triggering with *PD-1* blockade because of the high level of immune infiltration in these tumors.

Concomitant GITR triggering or BTLA blockade enhances antitumor activity of PD-1 blockade or chemotherapy in murine ESCC models

Accumulating evidence has shown that agonists of GITR or targeting BTLA have considerable potential to induce antitumor responses and complement the currently available ICB.[30] We next validated the efficacy of anti-GITR agonist antibody/anti-PD-1 antibody and anti-BTLA antibody/anti-PD-1 antibody in syngeneic mouse models of ESCC. MEC25 cells were inoculated subcutaneously into C57BL/6 mice. One week later, the mice were randomly divided into four groups and administered either isotype IgG control, or anti-GITR antibody alone, or anti-PD-1 antibody alone, or the combination of anti-GITR antibody and anti-PD-1 antibody by intraperitoneal injection every three days. Twenty days after mEC25 cells were inoculated, tumors were excised and weighed. The combination therapy led to greater tumor inhibition than either anti-GITR or anti-PD-1 treatment alone (Fig. 5a). We also assessed the effects of the combination of anti-BTLA and anti-PD-1 on immunocompetent ESCC mouse models. As expected, anti-BTLA enhanced anti-PD-1 treatment efficacy (Fig. 5b). Given that cisplatin-based chemotherapy has been the standard first-line treatment for ESCC, we also evaluated the effect of GITR triggering or BTLA blockade on DDP efficacy in mEC25 syngeneic mouse models. The results showed that triggering of GITR or blockade of BTLA significantly enhanced the treatment efficacy of DDP (Fig. 5c and d). To further characterize the effects of anti-GITR or anti-BTLA on the immune tumor microenvironment, we performed H&E staining experiments to evaluate the levels of tumor infiltrating lymphocytes (TILs) in syngeneic mice tumors treated with anti-BTLA antibody, anti-GITR agonist antibody and their respective isotype control. Both anti-BTLA antibody and anti-GITR agonist antibody significantly increased the levels of TILs (Figure S4a and b). To assess the potential role of T cell exhaustion in anti-GITR or anti-BTLA treatment, we also examined the percentage of PD1+CD8+ T (Tex) cells isolated from mice tumors by flow cytometry. Both treatment had no effect on the percentage of Tex (Figure S4c). Considering all these findings, we propose effective combination strategies for ESCC.

(4 Gy) (d) at the indicated times. Scale bars, 5 μm. (e) KYSE30 and KYSE450 cells were transfected with siRNAs targeting HFM1 and control siRNAs and then treated with 2 μg/ml DDP. The expression of HFM1 and γH2AX was analyzed by Western blotting. (f) KYSE30 and KYSE450 cells were transfected with siRNAs targeting HFM1 and control siRNAs, exposed to X-IR (4 Gy), and harvested at the indicated times. The expression of HFM1 and γH2AX was analyzed by Western blotting. (g, h) Representative pictures and quantification analysis of γH2AX foci in HFM1-depleted KYSE410 and KYSE450 cells and control cells treated with 2 μg/ml DDP (g) or X-IR (4 Gy) (h) at the indicated times. Scale bars, 5 μm. Data in c and d and g and h are representative of three independent experiments and represent the mean ± SD. Each dot represents a single cell, and ImageJ was used to count 50 cells in each group for this experiment. P values were determined by the Mann–Whitney U test.

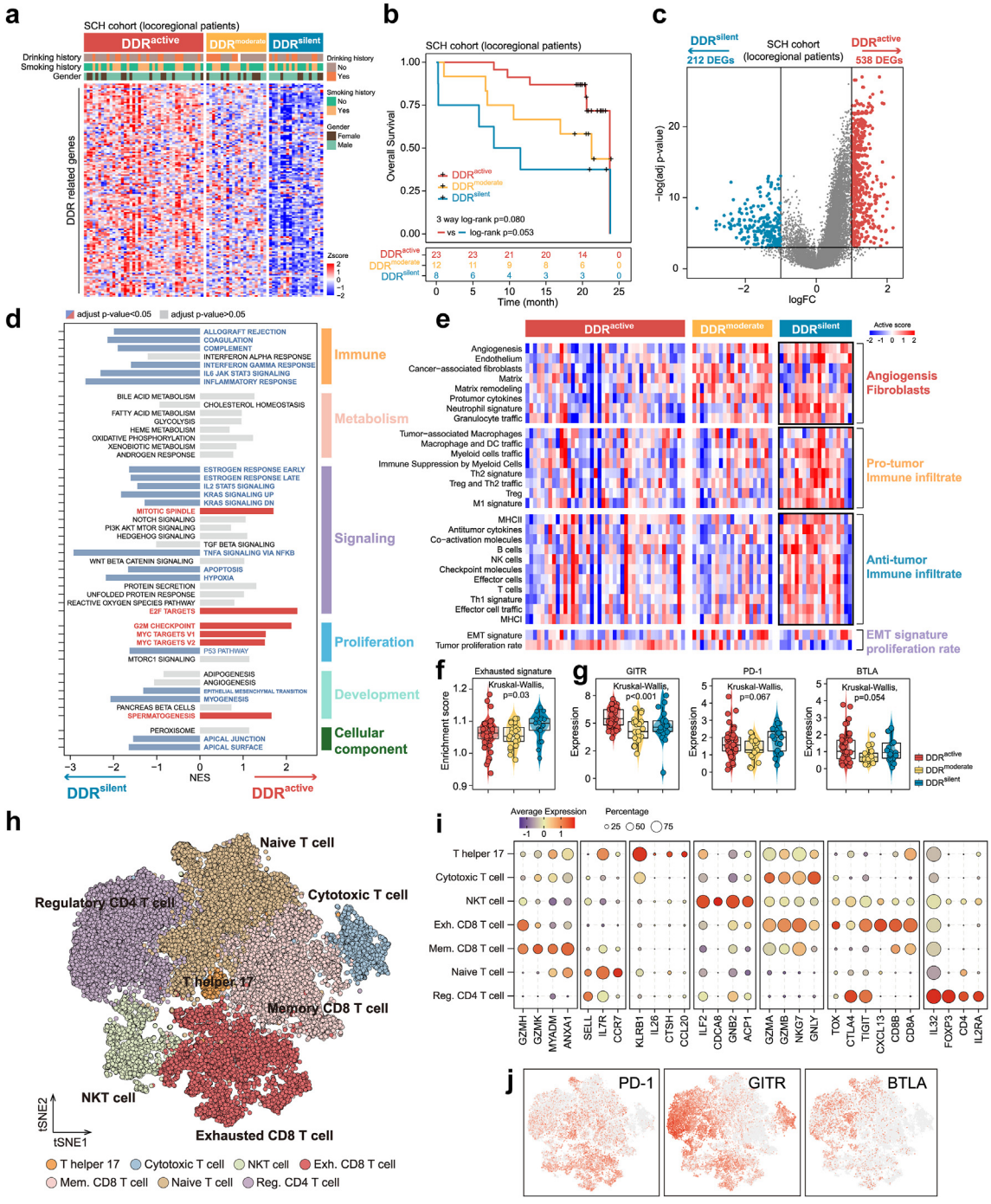

Fig. 4: **Immune microenvironment characterization of DDR subtypes identified GITR and BTLA as potential targets for immunotherapy.** (a) Heatmap of the expression fold changes in DDR genes among DDR subtypes in locoregional ESCC patients. The red bar represents the DDR^{active} subtype, the yellow bar represents the DDR^{moderate} subtype, and the green bar represents the DDR^{silent} subtype. The DDR subtypes are classified by the consensus clustering method. (b) Kaplan–Meier curves comparing OS among the DDR^{active} subtype, DDR^{moderate} subtype and DDR^{silent} subtype in locoregional ESCC patients (log-rank test P = 0.053). (c) Volcano plot showing genes that are differentially expressed between the DDR^{active} subtype and DDR^{silent} subtype (DDR^{active} vs. DDR^{silent}). Red points represent overexpressed DEGs in the DDR^{active} subtype, and blue points represent 212 underexpressed DEGs in the DDR^{silent} subtype. Gray points represent insignificant DEGs. The P value was calculated by empirical Bayes moderation from limma. (d) Bar plot showing the enrichment level of 50 hallmark gene sets between the DDR^{active} subtype and DDR^{silent} subtype. Red bars represent the significantly enriched hallmark gene sets in DDR^{active}. Blue bars represent the significantly

Discussion

This study provides the most comprehensive characterization of DDR gene expression in a Chinese ESCC cohort with clinical follow-up data. We classified 155 ESCC patients into DDRactive and DDRsilent classes based on the expression of DDR genes. Integrative analysis of clinical features revealed ESCC DDRactive and DDRsilent subtypes that may robustly predict patient outcomes in locoregional ESCC patients but not in metastatic ESCC patients, suggesting that DDR molecular features are unique and specific for locoregional ESCC. Notably, the prognosis of locoregional ESCC patients with DDRsilent features is worse than that of metastatic ESCC patients, suggesting a great need for clinical treatment options after esophagectomy for these patients.

Despite recent advancements in characterizing the molecular features of ESCC, there remains a scarcity of clinically relevant biomarkers for locoregional ESCC. In this study, we uncovered low *BRCA1* and high *HFM1* expression as independent prognostic biomarkers for predicting poor survival in patients with locoregional ESCC based on the DDR subtype. In line with our findings, loss of *BRCA1* expression is associated with a poor prognosis in various cancer types.[31,32] HFM1, predominantly expressed in germ-line cells, is critical in crossover formation and complete synapsis of homologous chromosomes during meiosis. The variants of *HFM1* have been reported to be involved in the dysfunction of the reproductive system.[29,33] Furthermore, *HFM1* is an essential gene in MMR and increased expression of *HFM1* has been associated with a poor prognosis of ESCC.[34] We also identified high levels of *HFM1* as an independent risk factor in locoregional ESCC, reinforcing its role as a dominant gene regulating the DNA damage response. Functional assays confirmed that *BRCA1* promotes DDR, whereas *HFM1* suppresses DDR in ESCC cells. Hence, the aberrant expression of *BRCA1* or *HFM1* may improve the understanding of ESCC tumorigenesis and can be used to predict patient outcomes and guide treatment decisions for individuals with locoregional ESCC.

Pathway-level comparison analysis across DDR subtypes in our study showed that DDR^{active} tumors were enriched in gene sets annotated with *E2F* targets, *G2M* checkpoint and MYC targets, which are related to cell proliferation and play an important role in the process of tumorigenesis. DDR^{silent} tumors were enriched not only in canonical cancer-related pathways, including KRAS signaling and the P53 pathway, but also in immune response-related pathways, including the complement pathway IFN-γ response and the inflammatory response, suggesting that DDR deficiency may affect the interplay between tumor cells and their microenvironment. Intriguingly, DDR^{silent} tumors displayed higher immune infiltration levels, higher enrichment scores of TEX signal gene sets and higher *PD-1* expression levels than the other two DDR subtypes. These results suggest that the inflamed immune environment in DDR^{silent} tumors may be counterbalanced by an increase in immune checkpoint expression and the proportion of exhausted T cells, raising the possibility that *PD-1* blockade or immunotherapy combination strategies may be effective for DDR^{silent} tumors.

Among the differentially expressed immune checkpoints, the costimulatory receptor *GITR* and the coinhibitory receptor *BTLA* also attracted our special interest. *GITR* is widely recognized as an attractive target for immunotherapy.[35,36] It has been reported that *GITR* promotes the activation and proliferation of effector T cells and decreases the levels of regulatory T cells.[30,37] We found that *GITR* was highly expressed in regulatory CD4 T cells and cytotoxic T cells using single-cell sequencing data. Moreover, *GITR* exhibited a complementary expression pattern with *PD-1*, supporting that *GITR* triggering may exert a synergistic effect with *PD-1* blockade. *BTLA* is an inhibitory receptor of the immunoglobulin superfamily. BTLA and *PD-1* are related to and co-expressed on tumor antigen-specific CD8+ T cells. They possess the canonical immunoreceptor tyrosine-based inhibition motif (ITIM) and immunoreceptor tyrosine-based switch motif (ITSM) within the cytoplasmic tail.[38,39] Accordingly, *BTLA* can likely substitute for *PD-1* when *PD-1* is blocked.[40] Notably, it came to our attention that *BTLA* was expressed in many T-cell subpopulations and exhibited a similar expression pattern with *PD-1*, supporting that *BTLA* blockade may exert a synergistic effect with *PD-1* blockade. Based on this evidence, we propose immunotherapy strategies of concomitant *GITR* triggering or *BTLA* blockade with *PD-1* blockade for DDR^{silent} ESCC. Functional assays validated that anti-*PD-1*-based combination immunotherapy exerted effective antitumor activity in murine ESCC models. In addition, our results demonstrate that *GITR* triggering or *BTLA* blockade may promote anti-tumor immune responses by

enriched hallmark gene sets in DDR^{silent}. (e) Heatmap of the activity scores of 29 Fges among DDR subtypes in locoregional ESCC patients. (f, g) Box plots showing the distribution of immune checkpoint gene expression and exhausted T cell signature score among DDR subtypes (Kruskal–Wallis test). (h) T-distributed stochastic neighbor embedding (t-SNE) visualization of 7 T-cell clusters (32,918 T cells were collected from 31 locoregional ESCC patients) with specific markers, showing the annotation and color nodes for T-cell subpopulations in the tumor ecosystem. (i) Dot plot showing the expression of marker gene signatures of the seven T-cell subpopulations. Both color and size represent the effect size. (j) T-SNE visualization showing immune checkpoint gene expression in each T-cell subpopulation of locoregional ESCC.

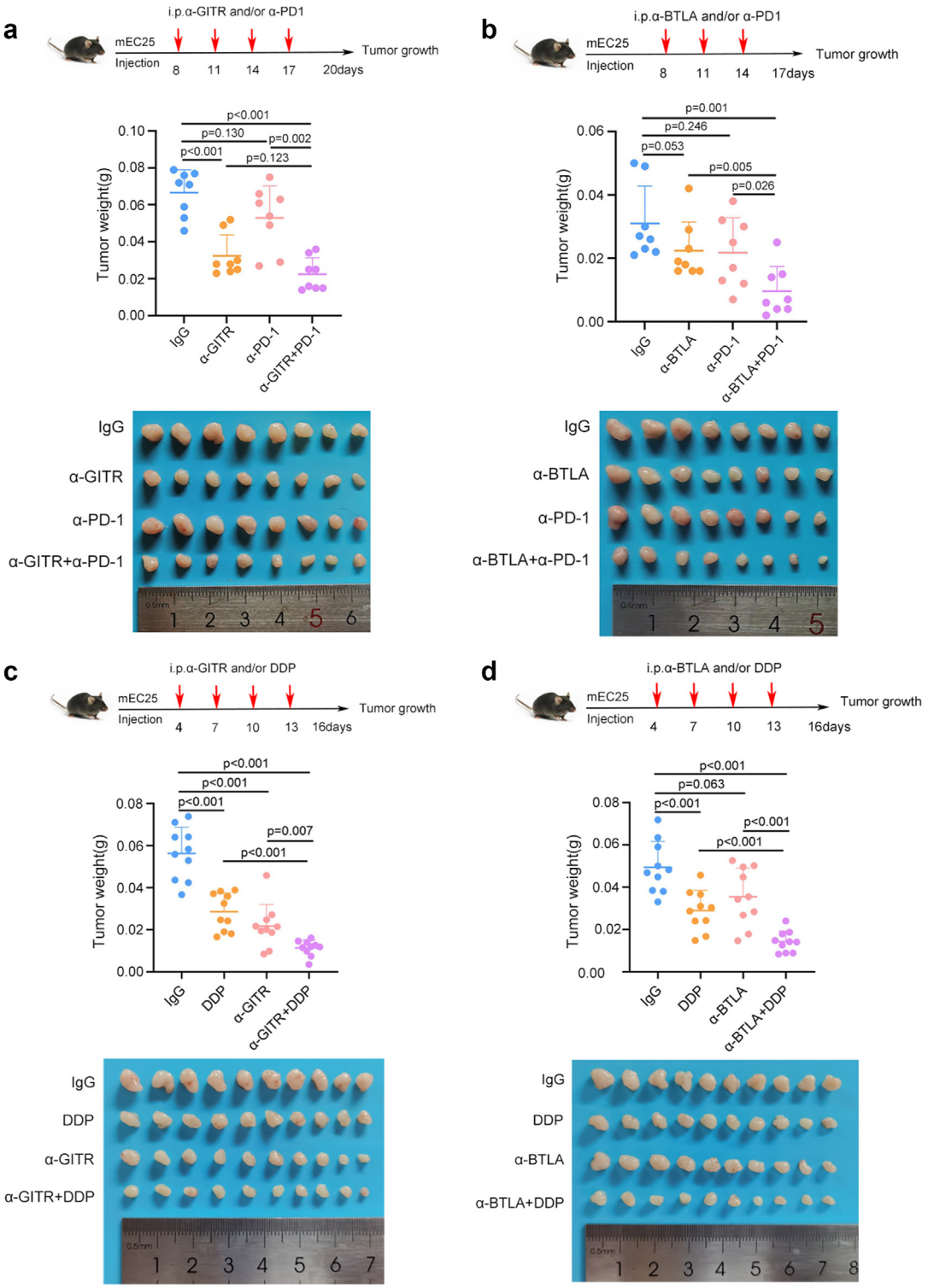

***Fig. 5:* GITR triggering or BTLA blockade potentiates the efficacy of anti-PD-1 antibody and cisplatin in murine ESCC models.** Schematic representation of the therapy schedule for α-GITR, α-PD-1, or combination therapy (a), for α-BTLA, α-PD-1, or combination therapy (b), for α-GITR, DDP, or combination therapy (c) and for α-BTLA, DDP, or combination therapy (d). Tumor images and the statistical results of tumor weights from syngeneic mEC25 models that received the indicated treatments (n = 8 in a and b, n = 10 in c and d). Data in a-d represent the mean ± SD and were analyzed by the Mann–Whitney U test.

increasing TILs levels. Additional mechanistic studies and clinical studies in larger patient cohorts are needed to validate this hypothesis.

Previous studies have shown that agonists of *GITR* and the blockade of *BTLA* have a potent therapeutic effect in other cancers, and the combination of *PD-1* blockade was even more effective.[36,37,41,42] However, there is limited evidence of either a response to therapy or clinical benefit from anti-*GITR*/anti-*BTLA* monotherapies, even in combinational therapies with anti-*PD-1*/*PD-L1*. This may be due to a lack of accurate biomarkers to select patients who may benefit.[30] Recent studies have shown that DDR status can be a potential biomarker to predict therapy response to ICB. For instance, the response to the *PD-1* inhibitor pembrolizumab could be predicted using the MMR status in patients with progressive metastatic carcinoma.[10,11] Deleterious mutations of several DDR-related genes were correlated with the clinical efficacy of pembrolizumab for non-small cell lung cancer.[43] HR defects have recently been identified as potential biomarkers to predict response to anti-*PD-1* therapy in various malignancies, including prostate and ovarian cancer.[44,45] Our study demonstrates that some locoregional ESCC patients with DDR^{silent} features may benefit from combinational immunotherapies. Moreover, we highlight the promising application of the DDR subtype in stratifying ESCC patients to guide immunotherapy selection.

In conclusion, our study highlights the value of DDR subtyping in the prognosis evaluation and clinical treatment of locoregional esophageal squamous cell carcinoma (ESCC) patients, offering a framework for more rational categorization of the disease and a foundation for the development of new therapies. Additionally, we demonstrated the potential of ICB-based treatment approaches beyond anti-*PD-1* antibodies in locoregional ESCC with DDR-silent features. These findings may pave the way for developing new therapeutic agents and clinical trials to improve outcomes for patients with locoregional ESCC.

Contributors

N. Zhao: Data curation, validation, investigation, methodology, writing-original draft, writing-review and editing. **Z. Zhang:** Data curation, validation, investigation, methodology, writing-original draft, writing-review and editing. **Q. Wang:** Data curation, validation, investigation and methodology. **L. Li:** Data validation, investigation and methodology. **Z. Wei:** Data curation, validation, methodology and writing-original draft. **H. Chen:** Conceptualization, data curation, formal analysis, supervision, validation, investigation, visualization, methodology, writing-original draft, writing-review and editing. **M. Zhou:** Conceptualization, data curation, formal analysis, supervision, validation, investigation, visualization, methodology, writing-original draft, writing-review and editing. **Z. Liu:** Conceptualization, supervision, writing-review and editing. **J. Su:** Conceptualization, methodology, supervision, writing-review and editing. All authors reviewed and approved the final version of the manuscript.

Data sharing statement

All ESCC RNA-seq data used in this study are publicly available from the Gene Expression Omnibus (GEO) database under accession numbers GSE53624 and GSE160269, Genome Sequence Archive (GSA) in the BIG Data Center (http://bigd.big.ac.cn/gsa) with the BioProject number PRJCA004501 and the UCSC Xena browser (https://xenabrowser.net/datapages/).

Declaration of interests

The authors have declared that no conflict of interest exists.

Acknowledgements

This study was supported by the National Key R&D Program of China (2021YFC2501000, 2022YFC3401003), the National Natural Science Foundation of China (82172882), the Beijing Natural Science Foundation (7212085), the CAMS Innovation Fund for Medical Sciences (2021-I2M-1-018, 2021-I2M-1-067), the Fundamental Research Funds for the Central Universities (3332021091), and the Non-profit Central Research Institute Fund of Chinese Academy of Medical Sciences (2019PT310027).

Appendix A. Supplementary data

Supplementary data related to this article can be found at https://doi.org/10.1016/j.ebiom.2023.104801.

References

1 Codipilly DC, Qin Y, Dawsey SM, et al. Screening for esophageal squamous cell carcinoma: recent advances. *Gastrointest Endosc*. 2018;88(3):413–426.
2 Kelly RJ. Emerging multimodality approaches to treat localized esophageal cancer. *J Natl Compr Canc Netw*. 2019;17(8):1009–1014.
3 Cui Y, Chen H, Xi R, et al. Whole-genome sequencing of 508 patients identifies key molecular features associated with poor prognosis in esophageal squamous cell carcinoma. *Cell Res*. 2020;30(10):902–913.
4 Zhou M, Bao S, Gong T, et al. The transcriptional landscape and diagnostic potential of long non-coding RNAs in esophageal squamous cell carcinoma. *Nat Commun*. 2023;14(1):3799.
5 Pearl LH, Schierz AC, Ward SE, Al-Lazikani B, Pearl FM. Therapeutic opportunities within the DNA damage response. *Nat Rev Cancer*. 2015;15(3):166–180.
6 Mouw KW, Goldberg MS, Konstantinopoulos PA, D'Andrea AD. DNA damage and repair biomarkers of immunotherapy response. *Cancer Discov*. 2017;7(7):675–693.
7 Howitt BE, Shukla SA, Sholl LM, et al. Association of polymerase e-mutated and microsatellite-instable endometrial cancers with neoantigen load, number of tumor-infiltrating lymphocytes, and expression of PD-1 and PD-L1. *JAMA Oncol*. 2015;1(9):1319–1323.
8 Chabanon RM, Muirhead G, Krastev DB, et al. PARP inhibition enhances tumor cell-intrinsic immunity in ERCC1-deficient non-small cell lung cancer. *J Clin Invest*. 2019;129(3):1211–1228.
9 Chabanon RM, Rouanne M, Lord CJ, Soria JC, Pasero P, Postel-Vinay S. Targeting the DNA damage response in immuno-oncology: developments and opportunities. *Nat Rev Cancer*. 2021;21(11):701–717.
10 Le DT, Uram JN, Wang H, et al. PD-1 blockade in tumors with mismatch-repair deficiency. *N Engl J Med*. 2015;372(26):2509–2520.
11 Le DT, Durham JN, Smith KN, et al. Mismatch repair deficiency predicts response of solid tumors to PD-1 blockade. *Science*. 2017;357(6349):409–413.
12 Bao S, Hu T, Liu J, et al. Genomic instability-derived plasma extracellular vesicle-microRNA signature as a minimally invasive predictor of risk and unfavorable prognosis in breast cancer. *J Nanobiotechnology*. 2021;19(1):22.
13 Knijnenburg TA, Wang L, Zimmermann MT, et al. Genomic and molecular landscape of DNA damage repair deficiency across the cancer genome Atlas. *Cell Rep*. 2018;23(1):239–254.e6.
14 Ronchetti L, Melucci E, De Nicola F, et al. DNA damage repair and survival outcomes in advanced gastric cancer patients treated with first-line chemotherapy. *Int J Cancer*. 2017;140(11):2587–2595.
15 Liu Z, Zhao Y, Kong P, et al. Integrated multi-omics profiling yields a clinically relevant molecular classification for esophageal squamous cell carcinoma. *Cancer Cell*. 2023;41(1):181–195.e9.
16 Li J, Chen Z, Tian L, et al. LncRNA profile study reveals a three-lncRNA signature associated with the survival of patients with oesophageal squamous cell carcinoma. *Gut*. 2014;63(11):1700–1710.

17 Zhang X, Peng L, Luo Y, et al. Dissecting esophageal squamous-cell carcinoma ecosystem by single-cell transcriptomic analysis. *Nat Commun*. 2021;12(1):5291.
18 Huang T, Yang J, Liu B, Fu L. A new mouse esophageal cancer cell line (mEC25)-derived pre-clinical syngeneic tumor model for immunotherapy. *Cancer Commun (Lond)*. 2020;40(7):316–320.
19 Wilkerson MD, Hayes DN. ConsensusClusterPlus: a class discovery tool with confidence assessments and item tracking. *Bioinformatics*. 2010;26(12):1572–1573.
20 Ritchie ME, Phipson B, Wu D, et al. Limma powers differential expression analyses for RNA-sequencing and microarray studies. *Nucleic Acids Res*. 2015;43(7):e47.
21 Liberzon A, Birger C, Thorvaldsdottir H, Ghandi M, Mesirov JP, Tamayo P. The Molecular Signatures Database (MSigDB) hallmark gene set collection. *Cell Syst*. 2015;1(6):417–425.
22 Wu T, Hu E, Xu S, et al. clusterProfiler 4.0: a universal enrichment tool for interpreting omics data. *Innovation (Camb)*. 2021;2(3):100141.
23 Hanzelmann S, Castelo R, Guinney J. GSVA: gene set variation analysis for microarray and RNA-seq data. *BMC Bioinformatics*. 2013;14:7.
24 Chen DS, Mellman I. Elements of cancer immunity and the cancer-immune set point. *Nature*. 2017;541(7637):321–330.
25 Senbabaoglu Y, Gejman RS, Winer AG, et al. Tumor immune microenvironment characterization in clear cell renal cell carcinoma identifies prognostic and immunotherapeutically relevant messenger RNA signatures. *Genome Biol*. 2016;17(1):231.
26 Zheng Y, Chen Z, Han Y, et al. Immune suppressive landscape in the human esophageal squamous cell carcinoma microenvironment. *Nat Commun*. 2020;11(1):6268.
27 Hao Y, Hao S, Andersen-Nissen E, et al. Integrated analysis of multimodal single-cell data. *Cell*. 2021;184(13):3573–3587.e29.
28 Tarsounas M, Sung P. The antitumorigenic roles of BRCA1-BARD1 in DNA repair and replication. *Nat Rev Mol Cell Biol*. 2020;21(5):284–299.
29 Wang J, Zhang W, Jiang H, Wu BL, Primary Ovarian Insufficiency C. Mutations in HFM1 in recessive primary ovarian insufficiency. *N Engl J Med*. 2014;370(10):972–974.
30 Kraehenbuehl L, Weng CH, Eghbali S, Wolchok JD, Merghoub T. Enhancing immunotherapy in cancer by targeting emerging immunomodulatory pathways. *Nat Rev Clin Oncol*. 2022;19(1):37–50.
31 Zhang ZZ, Liu YJ, Yin XL, Zhan P, Gu Y, Ni XZ. Loss of BRCA1 expression leads to worse survival in patients with gastric carcinoma. *World J Gastroenterol*. 2013;19(12):1968–1974.
32 Paik ES, Chang CS, Chae YL, et al. Prognostic relevance of BRCA1 expression in survival of patients with cervical cancer. *Front Oncol*. 2021;11:770103.
33 Yu L, Li M, Zhang H, et al. Novel pathogenic splicing variants in helicase for meiosis 1 (HFM1) are associated with diminished ovarian reserve and poor pregnancy outcomes. *J Assist Reprod Genet*. 2022;39(9):2135–2141.
34 Yuan H, Qing T, Zhu S, et al. The effects of altered DNA damage repair genes on mutational processes and immune cell infiltration in esophageal squamous cell carcinoma. *Cancer Med*. 2023;12(8):10077–10090.
35 Ko K, Yamazaki S, Nakamura K, et al. Treatment of advanced tumors with agonistic anti-GITR mAb and its effects on tumor-infiltrating Foxp3+CD25+CD4+ regulatory T cells. *J Exp Med*. 2005;202(7):885–891.
36 Zappasodi R, Sirard C, Li Y, et al. Rational design of anti-GITR-based combination immunotherapy. *Nat Med*. 2019;25(5):759–766.
37 Sukumar S, Wilson DC, Yu Y, et al. Characterization of MK-4166, a clinical agonistic antibody that targets human GITR and inhibits the generation and suppressive effects of T regulatory cells. *Cancer Res*. 2017;77(16):4378–4388.
38 Watanabe N, Gavrieli M, Sedy JR, et al. BTLA is a lymphocyte inhibitory receptor with similarities to CTLA-4 and PD-1. *Nat Immunol*. 2003;4(7):670–679.
39 Riley JL. PD-1 signaling in primary T cells. *Immunol Rev*. 2009;229(1):114–125.
40 Celis-Gutierrez J, Blattmann P, Zhai Y, et al. Quantitative interactomics in primary T cells provides a rationale for concomitant PD-1 and BTLA coinhibitor blockade in cancer immunotherapy. *Cell Rep*. 2019;27(11):3315–33130.e7.
41 Lu L, Xu X, Zhang B, Zhang R, Ji H, Wang X. Combined PD-1 blockade and GITR triggering induce a potent antitumor immunity in murine cancer models and synergizes with chemotherapeutic drugs. *J Transl Med*. 2014;12:36.
42 Wang B, Zhang W, Jankovic V, et al. Combination cancer immunotherapy targeting PD-1 and GITR can rescue CD8(+) T cell dysfunction and maintain memory phenotype. *Sci Immunol*. 2018;3(29):eaat7061.
43 Rizvi NA, Hellmann MD, Snyder A, et al. Cancer immunology. Mutational landscape determines sensitivity to PD-1 blockade in non-small cell lung cancer. *Science*. 2015;348(6230):124–128.
44 Sharma P, Pachynski RK, Narayan V, et al. Nivolumab plus ipilimumab for metastatic castration-resistant prostate cancer: preliminary analysis of patients in the CheckMate 650 trial. *Cancer Cell*. 2020;38(4):489–499.e3.
45 Farkkila A, Gulhan DC, Casado J, et al. Immunogenomic profiling determines responses to combined PARP and PD-1 inhibition in ovarian cancer. *Nat Commun*. 2020;11(1):1459.